Biosensors and Bioelectronics 167 (2020) 112504

Contents lists available at ScienceDirect

Biosensors and Bioelectronics

journal homepage: http://www.elsevier.com/locate/bios

Three-dimensional biosensor surface based on novel thorns-like polyelectrolytes

Wenwei Pan, Ziyu Han, Ye Chang, Xuexin Duan *

State Key Laboratory of Precision Measuring Technology & Instruments, College of Precision Instrument and Opto-electronics Engineering, Tianjin University, Tianjin, 300072, China

ARTICLE INFO

Keywords:
Biosensor
Antifouling
Immunosensing
Polyelectrolytes

ABSTRACT

We have developed a new three-dimensional (3D) surface for use in biosensors that is based on modified novel thorns-like polyelectrolytes (3D-PETx), which comprises of poly-*L*-lysine (PLL) appended with multitude oligo (ethylene glycol) (OEG) and biotin moieties. It tethered to the sensor surface by PLL, while the OEG-biotin chains are forced to stretch away from the surface for target detections. Due to its 3D structure, the number of the OEG-biotin per surface unit is markedly increased compared to conventional 2D polyelectrolytes (2D-PET) coating. Their antifouling property and sensing performance for human IgG and PSA were compared with the 2D-PET by BioLayer Interferometry (Blitz), Surface Plasmon Resonance (SPR), microfluidic devices and Enzyme-Linked ImmunoSorbent Assay (ELISA). Experimental results show that 3D-PETx presents higher sensitivity for biomarker detection both in buffer and in serum and provides an almost non-fouling surface even in undiluted serum. In addition, a sensitive PSA detection was achieved in undiluted serum with a LOD down to 0.6 ng/mL. The successful immunosensing in undiluted serum demonstrate the potential of the 3D-PETx coating for real clinical applications.

1. Introduction

Affinity biosensors have been widely used in medical diagnosis, food industry, pharmaceutical, agricultural, and environmental applications (Sappia et al., 2018; Mcpartlin et al., 2017; Jiang et al., 2018; Wei et al., 2020; Dieu et al., 2018; Matta et al., 2018). Such biosensors typically require immobilization of biomolecules onto the solid sensor surfaces as probes to achieve specific bio-recognitions, which is one of the most critical steps in the fabrication of high-performance biosensors (Burg et al., 2007; Srivastava et al., 2017). An idea biosensor surface will maintain the high binding capacity and specificity of the surface immobilized biomolecules, while minimize the interference from other molecules (e.g. reduce the nonspecific bindings (NSB)). Many surface chemistry has been developed for this end. Thiol derivatives (Love et al., 2005), silane agents (Howarter et al., 2006), and phosphonate agents (Albrecht-Schmitt et al., 2011) have been developed to form self-assembled monolayers (SAMs) on gold, silicon dioxide and other metal oxides surfaces to achieve the first step surface activation, followed by further immobilization of bio-probes through covalent binding. Although these approaches are well established for this purpose, they cannot achieve a good control of the surface activation (e.g. the surface density of the probes, the regeneration of the surface) due to the limitations of the SAMs reactions.

Activation of the biosensor surface using polymer coatings, such as functionalized polyethylene glycol (PEG), polysaccharide, and amphoteric ionic polymers etc. have been developed as well (Kingshott et al., 2002; Jonkheijm et al., 2008; Singh et al., 1999; Howarter et al., 2006). Compared with the SAMs, the solution synthesized polymers facilitate the design of their functional group densities, antifouling, and surface regeneration properties. Among all these polymers, polyelectrolytes based brush like copolymers have attracted a lot research interests (Zhang et al., 2011; Park et al., 2010). In such a system, cationic polyelectrolytes (e.g. Poly-*L*-lysine (PLL)) are usually functionalized as the polymer backbone, where bio-functional groups (e.g. biotin) terminated PEGs are grafted to these polyelectrolytes as sidechains (Zhen et al., 2004; Marie et al., 2006; Morgenthaler et al., 2006). When applied to surface, the positively charged polyelectrolytes will assembly to the negatively charged substrates (e.g. gold, silicon dioxide etc.) as a monolayer fashion, through reversible physisorption governed by the number of contact points between the polyelectrolytes and the interface. Their surface tethering is sufficiently dense, that the side PEG chains are forced to stretch away from the surface along the direction normal to the

* Corresponding author.
E-mail address: xduan@tju.edu.cn (X. Duan).

https://doi.org/10.1016/j.bios.2020.112504
Received 14 July 2020; Received in revised form 5 August 2020; Accepted 6 August 2020
Available online 13 August 2020
0956-5663/© 2020 Elsevier B.V. All rights reserved.

grafting surface to enable the bio-functionalization of the sensor, while maintaining their antifouling property due to their hydrophilicity (Gregory et al., 2000; Ruiz-Taylor et al., 2001). Since the polymers were prepared in solution, the surface densities of the bio-functional groups can be well controlled by designed chemistry at the molecular level. Recently, the long PEG side chains have been replaced by short oligo-ethylene glycol (OEG) (Duan et al., 2015). It has the advantages of preventing the back-folding of the front PEG side chains, which may reduce the binding capacities of the functionalized groups, while keeping its protein-resistant ability simultaneously. Later, maleimide and thiol click chemistry have been used as the end functional groups of OEG to enable the oligonucleotide sensing through such interface (Veerbeek et al., 2018; Iorio et al., 2019).

Though the polyelectrolytes conjugated with the linear PEG/OEG side chain provide a well-defined biosensor surface with versatile and precisely controlled sensor surface functional group densities, the binding capacity of such coating is still limited. This is due to the surface self-assembly polymer monolayer only provides a typical two-dimensional (2D) interface. It has limited biomolecule binding sites, which is controlled by the PEG/OEG graft density. The number of contact points between the polyelectrolytes and the interface should be maintained high enough to ensure their surface binding stability, thus the side chain graft density cannot easily be increased (Duan et al., 2015). Besides, due to sterical hindrance on the flat extended monolayer, there is only a fraction of the end functional groups will be able to react with the targets or probe molecules. Thus, the total number of reaction sites per sensor surface unit is rather limited in the real sensing applications, where it is desirable to immobilize an increased amount of probe molecules on a surface.

To solve this issue, in this work, we designed and synthesized a novel thorns-like three-dimensional (3D) polyelectrolyte copolymer (3D-PETx), which comprises of a linear positively charged PLL backbone, grafted with multiple brush-like OEG-biotins as side chains. Compared to the reported 2D polyelectrolyte copolymer (2D-PET) with chain-end biotin units, the 3D-PETx coating can generate a 3D surface with multitude biotin groups at different controlled latitude, thus the number of molecules interacting per surface unit is markedly increased. The end functionalized biotin units can specifically interact with streptavidin (SAv) and further link with biotinylated-proteins, which can be used to detect various biomarkers. Three different 3D-PETx were designed with varied grafting ratio of the OEG-biotin sidechains (10%, 30% and 40%). They were tested as biosensor surface on different substrates. Their antifouling property and sensing performance for SAv, human IgG and PSA were compared with the 2D-PET by interferometry, SPR, microfluidic devices and ELISA both in buffer and serum.

2. Materials and methods

2.1. Materials

Poly-*L*-lysine hydrobromide (PLL, MW = 15 kDa–30 kDa) and streptavidin labeled with fluorescein isothiocyanate (Streptavidin-FITC) were purchased from Sigma-Aldrich (USA). NHS-PEG_{12}-Biotin, NHS-PEG_4-Methyl, NHS-PEG_4-Alkynyl were purchased from Ponsure Biotechnology (Shanghai, China). PLL-N_3 was purchased from Nanosoftpolymers (USA). Streptavidin was purchased from Aladdin Industrial Corporation (Shanghai, China). Human IgG and biotinylated anti-human IgG were purchased from NNCrystal (Hangzhou, China). Human prostate specific antigen and biotinylated antibody to human prostate specific antigen (bio-tinylated anti-PSA) and PSA ELISA kit were purchased from Linc-Bio (Shanghai, China). The chemicals were used directly without further purifications. The SAv-FITC, SAv, Human IgG, and anti-human IgG solutions involved in the bioassay all use 10 mM HEPES buffer (pH 7.4) as a solvent.

2.2. Synthesis of polymers

Synthesis of PLL-*g*-PEG_{12}-Biotin was accomplished by reaction between NHS-OEG_{12}-Biotin and PLL (15–30 kDa). First, PLL-N_3 was dissolved in 50 × 10^{-3} M sodium carbonate buffer (pH 8.5) at a concentration of 40 mg/mL. The solution was filtered through a 220 nm pore syringe filter. Solid NHS-PEG_{12}-biotin was added to the dissolved PLL solution in the desired stoichiometric ratio (40%) under vigorous stirring. The reaction was proceeded for 8 h at room temperature, after which the aqueous solution was placed into a 3 kDa molecular weight cutoff Amicon Ultra centrifugal filter device (Millipore, USA) and centrifuged at 8.5 Kg for 20 min followed by washing the filter with DI water. The centrifugation and wash process were repeated 3 times to completely remove the ions in copolymer solution. The purified solution was lyophilized for 48 h and stored in freezer. The chemical structure of PLL-*g*-PEG_{12}-Biotin was verified by (NMR). (^{1}H NMR in D_2O (see also the Supplementary Information). δ [ppm] = 1.33–1.44 (lysine γ –CH_2), (biotin, β –CH_2-), 1.46–1.88 (lysine β, δ-CH_2), (biotin, γ –CH_2), 2.14 (biotin, –CH_2 C(O)NH-), 2.53 (coupled PEG, –CH_2 –C(O)–N), 2.69 (lysine,(–CH_2–C(O)–N)), 2.81–2.87 (lysine, –CH_2-NH-C(O)), (PEG,–CH_2–NH-C(O)), 3.06 (biotin, -S–CH_2–), 3.21 (biotin, -S–CH–), 3.26(free lysine, -N-CH_2), 3.57 (PEG, CH_2 –O-), 4.13 (lysine, N–CH–C(O)-),4.28 and 4.46 (biotin, 2 bridge head CH)).

Synthesis of 2D-POBWPA was accomplished by reaction of NHS-PEG_{12}-biotin with PLL-N_3 (3 kDa). First, PLL-N_3 was dissolved in 50 × 10^{-3} M sodium carbonate buffer (pH 8.5) at a concentration of 40 mg/mL. The solution was filtered through a 220 nm pore syringe filter. Solid NHS-OEG_{12}-biotin was added to the dissolved PLL-N_3 solution in the desired stoichiometric ratio (30%) under vigorous stirring. The reaction was proceeded for 8 h at room temperature. Then, excess NHS-PEG_4-Methyl was added to the solution and stirred for another 8 h, after which the aqueous solution was placed into a 3 kDa molecular weight cutoff Amicon Ultra centrifugal filter device (Millipore, USA) and centrifuged at 8.5 Kg for 20 min followed by washing the filter with DI water. The centrifugation and wash process were repeated 3 times to completely remove the ions in copolymer solution. The purified solution was lyophilized for 48 h and stored in freezer. The chemical structure of 2D-POBWPA was verified by (NMR). (^{1}H NMR in D_2O (see also the Supplementary Information). δ [ppm] = 1.34–1.43 (lysine γ –CH_2), (biotin, β –CH_2-), 1.47–1.87 (lysine β, δ-CH_2), (biotin, γ –CH_2), 2.15 (biotin, –CH_2 C(O)NH-), 2.51 (coupled PEG, –CH_2 –C(O)–N), 2.68 (lysine, (–CH_2–C(O)–N)), 2.82–2.89 (lysine, –CH_2-NH-C(O)), (PEG,–CH_2–NH-C(O)), 3.07 (biotin, -S–CH_2–), 3.21 (biotin, -S–CH–), 3.27(free lysine, -N-CH_2), 3.38 (PEG,-O-CH3), 3.56 (PEG, CH_2 –O-), 4.13 (lysine, N–CH–C(O)-),4.27 and 4.45 (biotin, 2 bridge head CH)).

Synthesis of 2D-POBWPA-NHS was accomplished by copper-catalyzed click chemistry. First, CuI (0.0019 g, 1 mol %) was added to 1 g of water under air. Then, 2D-POBWPA (1 mmol) and NHS-PEG_4-Alkynyl (1 mmol) were added to the reaction mixture at room temperature and stirred for 2 h. After this, the solution was filtered through a 220 nm pore syringe filter, after which the aqueous solution was placed into a 3 kDa molecular weight cutoff Amicon Ultra centrifugal filter device (Millipore, USA) and centrifuged at 8.5 Kg for 20 min followed by washing the filter with DI water. The centrifugation and wash process were repeated 3 times to completely remove the ions in copolymer solution. The purified solution was lyophilized for 48 h and stored in freezer. The chemical structure of 2D-POBWPA was verified by (NMR). (^{1}H NMR in D_2O (see also the Supplementary Information). δ [ppm] = 1.32–1.41 (lysine γ –CH_2), (biotin, β –CH_2-), 1.48–1.89 (lysine β, δ-CH_2), (biotin, γ –CH_2), 2.16 (biotin, –CH_2 C(O)NH-), 2.52 (coupled PEG, –CH_2 –C(O)–N), 2.69 (lysine,(–CH_2–C(O)–N)), 2.83–2.91 (lysine, –CH_2-NH-C(O)), (PEG,–CH_2–NH-C(O)), 3.09 (biotin, -S–CH_2–), 3.23 (biotin, -S–CH–), 3.26(free lysine, -N-CH_2), 3.37 (PEG,-O-CH3), 3.55 (PEG, CH_2 –O-), 4.15 (lysine, N–CH–C(O)-),4.26 and 4.47 (biotin, 2 bridge head CH)).

Synthesis of 3D-PETx was accomplished by grafting 2D-POBWPA-

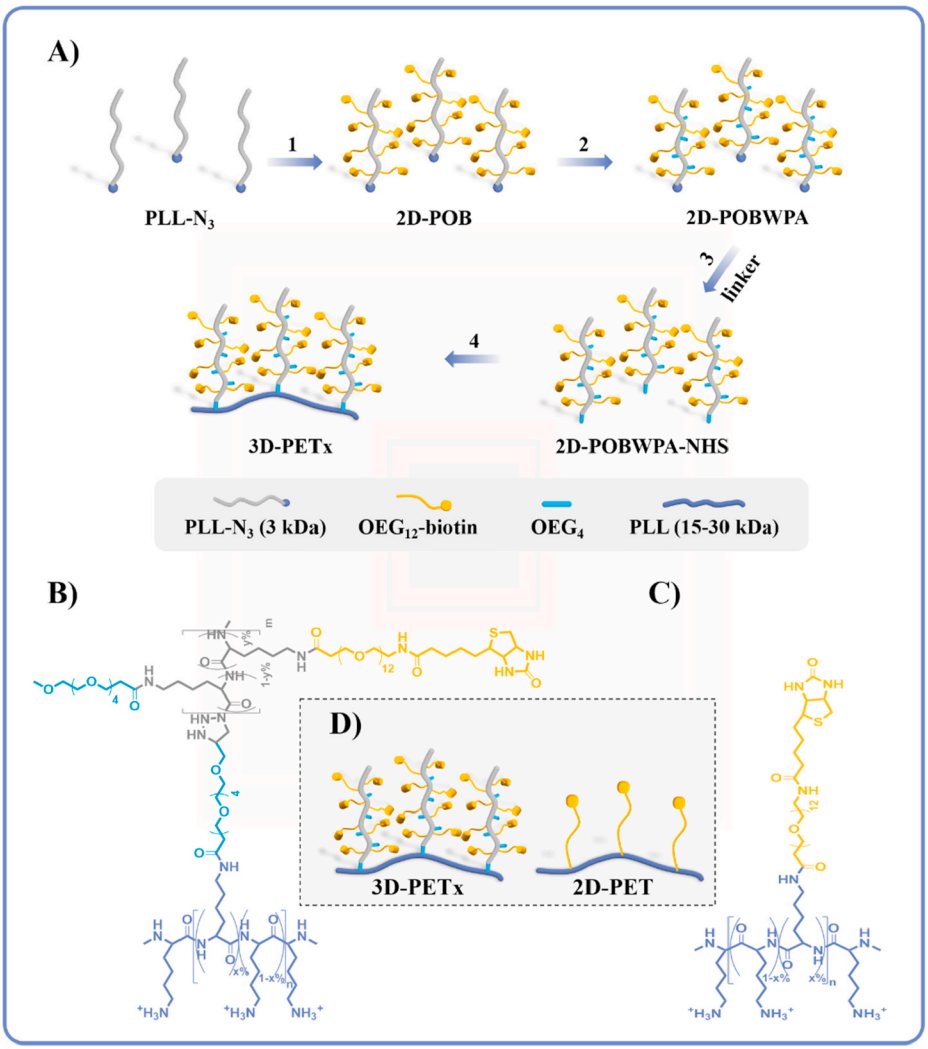

Fig. 1. Synthesis route A), chemical structure B) of 3D-PETx, chemical structure of 2D-PET C) and a comparison of 3D-PETx and 2D-PET D).

NHS to PLL (15–30 kDa) in the desired stoichiometric ratio (10%, 30% and 40%). The reaction conditions are the same as those of synthesis of 2D-POBWPA. After the reaction, the aqueous solution was placed into a 50 kDa molecular weight cutoff Amicon Ultra centrifugal filter device (Millipore, USA) and centrifuged at 8.5 Kg for 20 min followed by washing the filter with DI water. The centrifugation and wash process were repeated 3 times to completely remove the ions in copolymer solution. The purified solution was lyophilized for 48 h and stored in freezer. The chemical structure of 3D-PETx (10%) was verified by (NMR). (^{1}H NMR in D_2O (see also the Supplementary Information). δ [ppm] = 1.32–1.42 (lysine γ –CH_2), (biotin, β –CH_2-), 1.46–1.86 (lysine β, δ-CH_2), (biotin, γ –CH_2), 2.16 (biotin, –CH_2 C(O)NH-), 2.52 (coupled PEG, –CH_2 –C(O)–N), 2.69 (lysine,(–CH_2–C(O)–N)), 2.81–2.87 (lysine, –CH_2-NH-C(O)), (PEG,–CH_2–NH-C(O)), 3.06 (biotin, -S–CH_2–), 3.23 (biotin, -S–CH–), 3.28(free lysine, -N-CH_2), 3.39 (PEG,-O-CH3), 3.58 (PEG, CH_2 –O-), 4.15 (lysine, N–CH–C(O)-),4.28 and 4.47 (biotin, 2 bridge head CH)). The chemical structure of 3D-PETx (30%) was verified by (NMR). (^{1}H NMR in D_2O (see also the Supporting Information). δ [ppm] = 1.33–1.45 (lysine γ –CH_2), (biotin, β –CH_2-), 1.46–1.89 (lysine β, δ-CH_2), (biotin, γ –CH_2), 2.13 (biotin, –CH_2 C(O)NH-), 2.53 (coupled PEG, –CH_2 –C(O)–N), 2.69 (lysine,(–CH_2–C(O)–N)), 2.81–2.90 (lysine, –CH_2-NH-C(O)), (PEG,–CH_2–NH-C(O)), 3.09 (biotin, -S–CH_2–), 3.23 (biotin, -S–CH–), 3.29(free lysine, -N-CH_2), 3.41 (PEG,-O-CH3), 3.57 (PEG, CH_2 –O-), 4.15 (lysine, N–CH–C(O)-),4.29 and 4.43 (biotin, 2 bridge head CH)). The chemical structure of 3D-PETx (40%) was verified by (NMR). (^{1}H NMR in D_2O (see also the Supporting Information). δ [ppm] = 1.34–1.42 (lysine γ –CH_2), (biotin, β –CH_2-), 1.44–1.89 (lysine β, δ-CH_2), (biotin, γ –CH_2), 2.13 (biotin, –CH_2 C(O)NH-), 2.54 (coupled PEG, –CH_2 –C(O)–N), 2.71 (lysine,(–CH_2–C(O)–N)), 2.84–2.92 (lysine, –CH_2-NH-C(O)), (PEG,–CH_2–NH-C(O)), 3.10 (biotin, -S–CH_2–), 3.23 (biotin, -S–CH–), 3.25(free lysine, -N-CH_2), 3.36 (PEG,-O-CH3), 3.57 (PEG, CH_2 –O-), 4.13 (lysine, N–CH–C(O)-),4.26 and 4.46 (biotin, 2 bridge head CH)).

2.3. Surface characterizations

All the fluorescent images were captured using an Olympus BX 53 microscope with an Olympus DP74 digital microscope camera. The AFM images (see the Supplementary Information) were obtained with a Bruker Icon AFM under tapping-mode using a silicon cantilever with a spring constant of 42 N/m and resonant frequency of 300 kHz. XPS measurements were performed in ultrahigh vacuum in an ESCALAB 250 Xi (Thermo Scientific) with a nominal spot size of 400 μm. Water contact angle was measured by JC2000DM.

2.4. BioLayer interferometry measurement

The PLL-Biotin based sensing scheme was verified by the ForteBio BioLayer Interferometry (BLItz) system (ForteBio Inc., USA). Blitz is a glass-fiber based biosensor which is based on the principle of optical

interferometry. The glass fiber tips were first cleaned in "piranha" solution (1:3 H_2O_2: H_2SO_4) before polyelectrolytes coating. PETs were assembled onto the glass tip followed by modifying with SAv and biotinylated antibody. The tips modified by the antibody are then used for antigen detection. The interference pattern shift was monitored as a function of time.

2.5. SPR analysis

SPR immunosensing experiments were performed using the P4SPR portable instrument (Affinité Instruments) (Zhao et al., 2015). It uses a SPR chip and a fluidic cell comprising three sensing channels and a reference channel. Thus, all samples were measured in triplicate. The dove prisms coated with gold were functionalized with the anti-PSA using the same method as Blitz. Before testing, 0.4 mL of blank human serum was injected over 20 min to passivate the surface. Human serum spiked with different concentrations of PSA (0.6, 2.5, 5, 10, 20, 40 ng/mL) (0.4 mL) was then injected and the binding was monitored for 10 min with each concentration.

2.6. ELISA test

The ELISA test was achieved using a commercial PSA ELISA kit. Firstly, 50 μL human PSA (0, 1, 4, 10, 25, 50 ng/mL) in 100% serum were added respectively to anti-PSA immobilized 96-well microplates initialized with our polyelectrolyte coatings, followed by incubation at 37 °C for 45 min and standard washing step. Then 100 μL HRP conjugated anti-PSA was added to each well and incubated for 45 min at 37 °C. After another washing step, 100 μL TMB substrate solution was added to each well and allowed to react under the condition of protection from light for 10 min at °C. 50 μL 2 M H_2SO_4 was then added immediately and the absorbance at 450 nm of each well was analyzed with a microplate reader (Multiskan GO, Thermo Scientific, USA).

3. Results and discussion

3.1. Design, synthesis, and characterizations of the 3D-PETx

In order to obtain the 3D structure, 3D-PETx was designed by grafting 2D PLL-*g*-OEG-biotin without primary amines (2D-POBWPA) as sidechains to a linear PLL backbone. Due to the positively charged PLL, 3D-PETx can physically absorbed to negatively charged substrate through strongly PLL-substrate interacting, while the other weakly interacting 2D-POBWPA blocks will stretch away from the surface. Thus, a full 3D thorns-like bio-functional surface is achieved (Fig. 1A).

To prepare such copolymer, the 2D-POBWPA side chains were synthesized as shown in Fig. 1A (steps 1–2). Firstly, the 2D-POB were prepared by reaction of NHS-OEG_{12}-biotins with a short linear PLL-N_3 (3 kDa, approximately 20 *L*-lysine units) with a terminal azide group with a controlled grafting ratio at 50%. In slightly basic conditions (pH = 7–9), NHS reacts efficiently with primary amino groups (-NH_2) of the lysine residues by nucleophilic attack, forming an amide bond and releasing the NHS group. Then, an excess amount of shorter chain length OEG (NHS-OEG_4-Melthys) was applied to cover the remaining amino groups on 2D-POB forming 2D-POBWPA, under the same reaction conditions (step 2). Here, different lengths of OEG chains (OEG_4 and OEG_{12}-biotin) were mixed for grafting to allow the protein binding sites (biotin) standing out, which can ensure their sufficiently exposure in aqueous solutions for specific bio-reactions. Next, in order to graft the side chain 2D-POBWPA onto the backbone PLL (15–30 kDa, approximately 150 *L*-lysine units) to obtain the 3D-PETx, we introduced the short-chain alkynyl-OEG_4-NHS as a hetero-linker. The main body of the linker consists of four oligo ethylene glycol units (OEG_4) with alkynyl and NHS at each end. The alkynyl end of the linker can be connected to 2D-POBWPA through copper-catalyzed click chemistry (step 3), after which the NHS end is connected to the PLL backbone through the reaction of primary amine and NHS mentioned above (step 4), thus forming the 3D-PETx (Fig. 1B). To compare with the 3D-PETx in subsequent sensing experiments, a typical 2D polyelectrolyte, PLL-*g*-OEG_{12}-biotin (2D-PET) is prepared as well, which has the same OEG_{12}-biotin components as 3D-PETx (Fig. 1C). Fig. 1D illustrates the intuitive comparison between 3D-PETx and 2D-PET.

Table 1
The polyelectrolytes used in this work and their selected physical properties after adsorption on Si/SiO_2 substrate (the water contact angle by three measurements using the same type of coating on different substrates).

Polymer name	x [%]	y [%]	OEG_{12}-biotin [%]	Water contact angle [°]
2D-PET	26.9	…	26.9	25.4 ± 2.1
3D-PETx (10%)	10.9	41.4	90.3	17.5 ± 1.7
3D-PETx (30%)	34	41.4	281.2	13.8 ± 2.4
3D-PETx (40%)	42.8	41.4	354.4	13.4 ± 2.7

Three 3D-PETx with different 2D-POBWPA graft ratios (the ratio of 2D-POBWPA grafted PLL to the total PLL units) were synthesized with 2D-POBWPA contents corresponding to x (%) = 10, 30, 40.^{1}H NMR was used to characterize the formation of such copolymers (Figs. S1–6). The final grafting ratio was determined from the relative areas of the lysine side-chain peak (-CH) at 4.14 ppm and the biotin peak (CH–N-) at 4.35 ppm in ^{1}H NMR. Table 1 shows the calculated real graft ratios of all the copolymers. It clearly proved that the formation of such copolymers and the content of 2D-POBWPA and OEG_{12}-biotin side chains agreed with the desired stoichiometric ratio. Besides the NMR, we characterized their behaviors on surface as well. At physiological pH, the 3D-PETx and 2D-PET are polycationic copolymers, which can absorb spontaneously to negatively charged substrate. Water contact angle (CA), AFM and XPS were then applied to characterize the copolymer thin films on flat silicon (Si/SiO_2) substrate. As shown in Table 1, as increased of the OEG_{12}-biotin content, the copolymer thin films become more hydrophilic, which is reflected in their gradually decreased of CA (Fig. S7). In general, we believe that OEG in OEG_{12}-biotin makes a significant contribution to the hydrophilicity of the thin films.

AFM was then applied to measure the morphology and thickness of the copolymer thin film. Fig. 2A shows that 3D-PETx (40%) forms a uniform thin film on the substrate, and the mean roughness (Ra) of film in the scan area (2.5 μm^2) is 0.218 nm. The measured thickness of 3D-PETx is about 8 nm (Fig. S8). XPS was conducted to determine the chemical composition of 3D-PETx (40%) coated silicon (Si/SiO_2) substrate. Fig. 2B shows that C, N, Si, and O are present on the substrate, of which C and N are from the copolymer thin film, Si is from the silicon substrate, and O is from the thin film and substrate. The respective contents of C, N and O are shown in Table S1. The measured ratio of C and N is 10.3: 1, which is very close to the theoretical value of the molecular design (9.4: 1). In Fig. 2c, the C 1s peak was split into four peaks at the binding energies of 284.7, 285.3, 286.3, and 288.1 eV, corresponding to C–C, C–N, C–O, and C═O, respectively. By comparing the respective proportions of these different types of C with theoretical values, the structure of the synthesized 3D-PETx is clearly confirmed (Table S1).

3.2. Streptavidin binding

To verify the surface assembling and bioactivities of the synthesized 3D-PETx, their binding performance for streptavidin (SAv) were compared with the 2D-PET monolayers in typical biosensors and microfluidic devices.

Here, Biolayer Interferometry (Blitz, Pall) which is a typical surface-based optical sensor was used. Any analyte adsorption at the very tip of the glass fiber will cause a shift of the interference wavelength, which is linear proportion to the amounts of absorbed molecules. Thus, Blitz can quantify the biomolecular surface interactions without labelling. Fig. 3a shows the schematic diagram of the SAv binding through

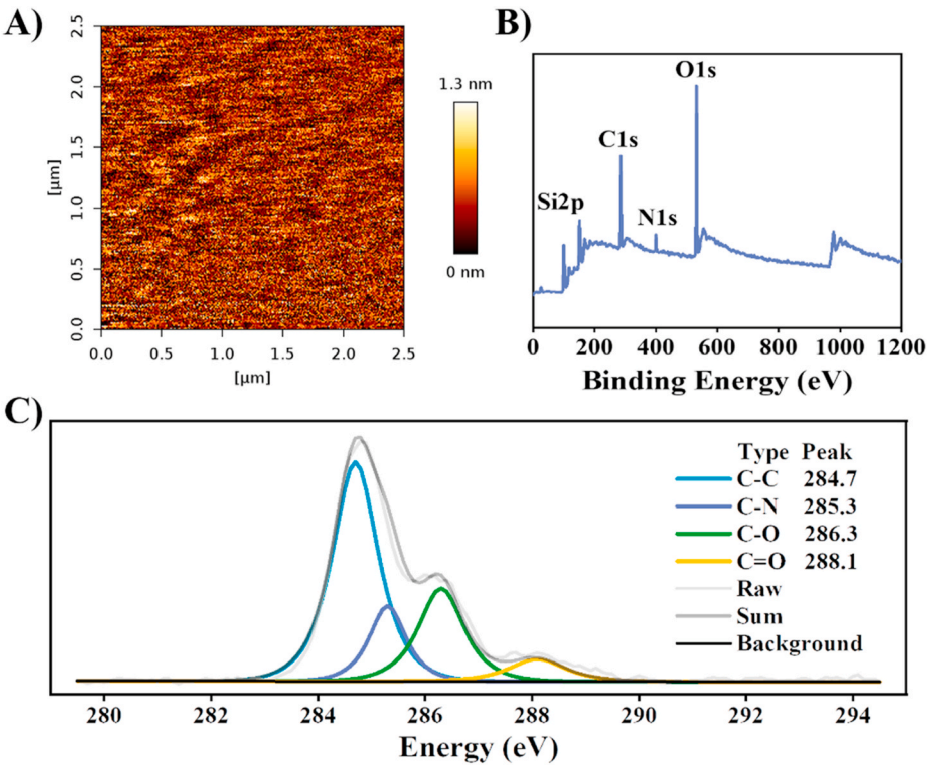

Fig. 2. AFM height image A), XPS survey spectra B), and XPS high resolution C1s spectra C) of 3D-PETx (40%) coating on Si/SiO_2 substrate.

polyelectrolytes surface assembling. After functionalization of the tips by the four polyelectrolyte solutions (three 3D-PETx with different biotin conjugation ratio and 2D-PET as a control), the tips were dipped into the same SAv solution (200 nM, 10 mM HEPES, pH7.4) for 300s followed by a through rinsing with HEPES buffer. As shown in Fig. 3b-c, SAv absorbed to all the four biotinylated polymers, all three 3D-PETx binding signals are much higher than the 2D-PET. This is due to that there are more OEG-biotin side chains on the 3D-PETx, which can provide more SAv binding sites.

To demonstrate the compatibility of the 3D-PETx coating, we then applied the same 3D-PETx and 2D-PET coatings into PDMS microfluidic channels and tested their SAv binding capacity using fluorescent labeled SAv. The polyelectrolyte solutions (1 mg/mL) were continuously injected into the same U-shaped PDMS channel (Fig. 3D) for 10 min. After buffer rinsing, FITC-SAv (200 nM) was injected into the channel to react with the biotin activated channels followed by rinsing with HEPES buffer to wash away the unbounded SAv. Their corresponding fluorescent intensities, which are proportional to the amount of the FITC-SAv immobilized on the PDMS channels were averaged and compared in Fig. 3E. Again, it clearly shows that the three 3D-PETx-modified channels have much higher fluorescence intensity compared to the 2D-PET, suggesting higher amount of SAv bindings. 3D-PETx with 40% graft ratio shows the highest SAv binding capacity. The results are rather comparable to the Blitz test. All these results demonstrated that the 3D-PETx coatings provide more numbers of reaction sites per sensor surface unit, which can immobilize more SAv compared to 2D-PET. Besides, such surface coating enables a rather stable coating, which can be applied to many different substrates. It is also noted that although the content of OEG_{12}-biotin in 3D-PETx (30%) and 3D-PETx (40%) is 3 and 4 times higher than that of 3D-PETx (10%), 3D-PETx (30%) and 3D-PETx (40%) did not show the expected overwhelming binding capacity for SAv. We hypothesized that this is due to the possibilities of undesired crosslinks between the OEG_{12}-biotin side chains, which connected by the symmetric SAvs (Fig. S9).

3.3. IgG detection

As a tetramer protein with symmetrical biotin binding sites, immobilized SAv can be used as a linker to further connect to other biotinylated antibodies for specific antigen detections (Han et al., 2017). Fig. 4A shows the schematic diagram of the sensing scheme of 3D-PETx activated sensor for IgG detections as a demonstration.

The human IgG detection based on the proposed four polyelectrolytes was carried out via Blitz. PETs (1 mg/mL), SAv (200 nM), and biotinylated anti-human IgG (200 μg/mL) were loaded by simply immersing the glass fiber tip into particular solutions in sequence to initialize the tips. The initialized glass tips were then exposed to 7 different concentrations of human IgG solutions over a range from 1 to 192 μg/mL. A washing step was involved to remove the unbounded analytes after each IgG incubation. Fig. 4b plots the wavelength shift as a function of IgG concentrations (see also the supplementary information for the real time measurement results, Fig. S10). It clearly shows that all three 3D-PETx showed higher sensitivity than 2D-PET. It proofs that the more numbers of biotin groups grafted at per sensor surface unit will provide more protein binding sites, which confirms the advantages to use 3D polyelectrolytes coating. It is also worth mentioning that 3D-PETx (40%) shows much better performance compared with other 3D-PETx. Although 3D-PETx may suffer side chain crosslinking by the bition-SAv (Fig. S9), the densely packed sidechains in 3D-PET (40%) has avoid some of the crosslinking, and the large effective SAv density makes 3D-PETx (40%) stand out in the detection of IgG.

As indicated above, further increasing grating percentage may lead to higher binding compacity, however we also need to consider their surface binding stability as the higher side chain grafting will result less PLL in the main backbone of the polymer. If the PLL backbone do not have enough protonated amines for surface bonding, it will influence their surface assembling stability. To ensure that PET has sufficient surface binding capacity, the grafting percentage was controlled below 40% (Ruiz-Taylor et al., 2001; Duan et al., 2015).

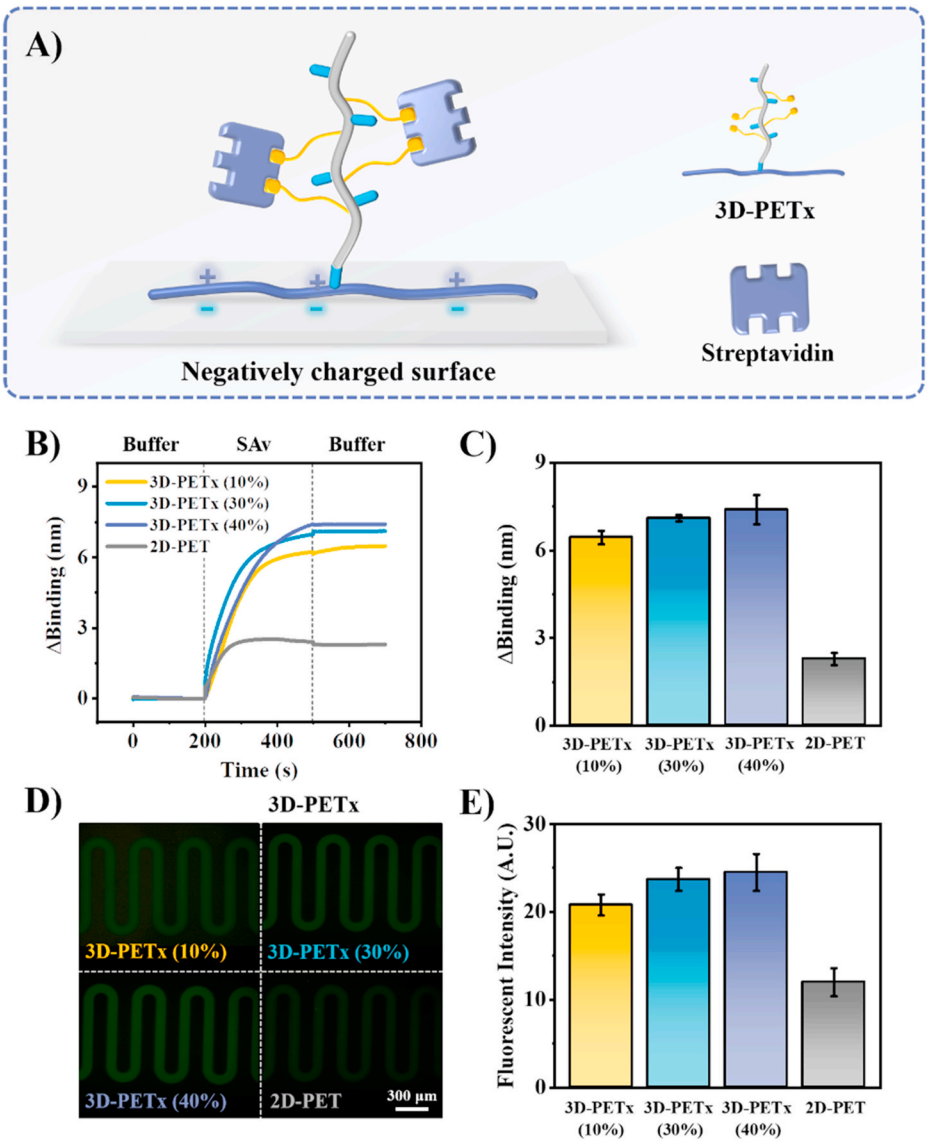

Fig. 3. A) The schematic diagram of the SAv binding through 3D-PETx surface assembling. Real time Blitz measurement B) and comparison of SAv bindings C) on different 3D-PETx and 2D-PET initialized glass fiber tip. Fluorescent images D), and the corresponding intensities E) of FITC-SAv bindings on different 3D-PETx and 2D-PET coated PDMS channels (100 μm in width). Error bars represent standard deviation, n = 4.

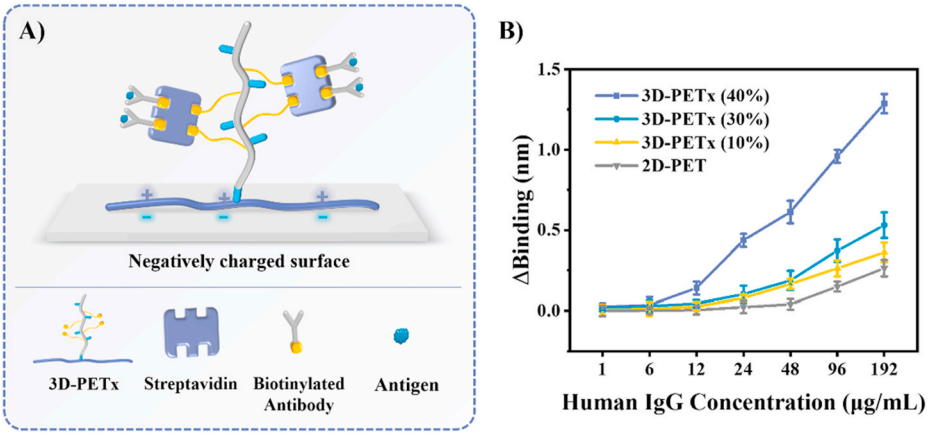

Fig. 4. A) The schematic diagram of IgG detections through 3D-PETx surface assembling and comparison of human IgG bindings B) over the concentration range from 1 μg/mL to 192 μg/mL on PETs initialized glass fiber tip. Error bars represent standard deviation, n = 4.

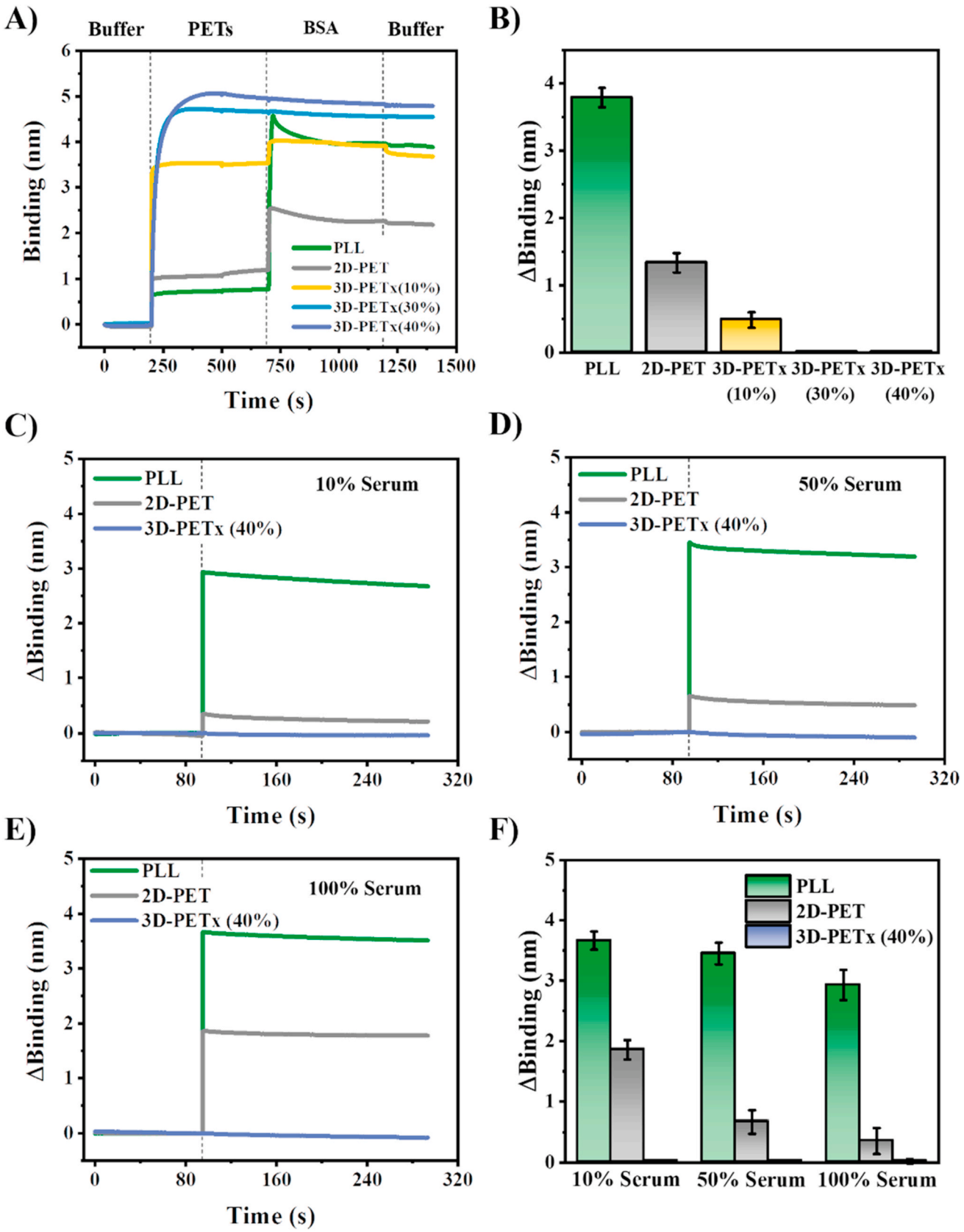

Fig. 5. (A) The monitored wavelength shift as a function of time for different polyelectrolytes initialized glass fiber tip for BSA adsorption using Blitz. (B) Comparison of BSA adsorption on different PETs initialized glass fiber tip. (C–E) The monitored baseline wavelength shift as a function of time for polyelectrolytes initialized glass fiber tips before and after serum treatment at different dilutions (10%, 50% and 100%) using Blitz. (F) Comparison of nonspecific adsorption on polyelectrolytes initialized glass fiber tip after serum treatment at different dilutions (10%, 50% and 100%). Error bars represent standard deviation, n = 4.

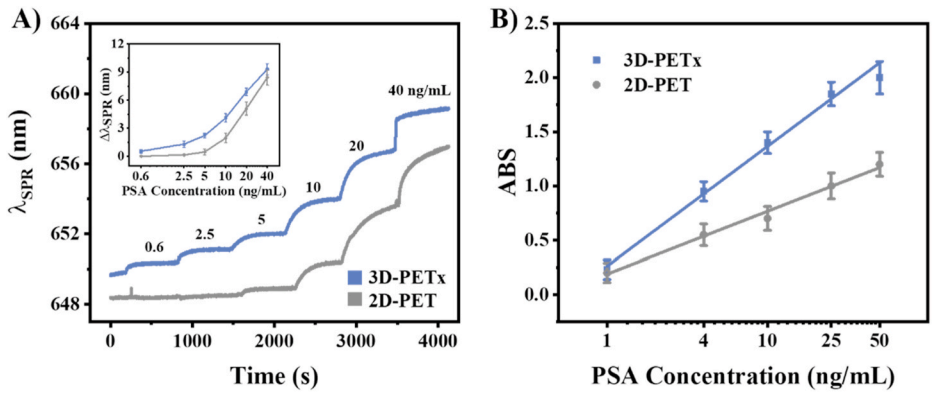

Fig. 6. A) SPR results for the detection of PSA in undiluted human serum. B) ELISA tests for PSA detection in undiluted serum. Error bars represent standard deviation, n = 4.

3.4. Anti-fouling test

The above results have confirmed the excellent performance of the 3D-PETx coating for protein detections. One of the major challenges in affinity biosensors for real medical applications is the non-specific bindings (fouling) of the clinically relevant biological fluids such as serum or plasma, which often leads to rapid loss of sensitivity (McKeating et al., 2019). Therefore, it is very important to develop anti-fouling coatings for biosensors. Poly (ethylene glycol) (PEG) (or oligo (ethylene glycol) (OEG)) (Gevrek et al., 2017; Andrea et al., 2015; Wu et al., 2019; Zhao et al., 2013) and zwitterionic materials (Chen et al., 2005; He et al., 2008; Lange et al., 2016) are two main materials that can effectively resist nonspecific protein adsorption from complex media and meet the challenges of biosensors (Prime et al., 1991). Since 3D-PETx has densely packed OEG side chains which can provide a rather hydrophilic surface, its anti-fouling ability is expected. To verify this, we used the Blitz platform to compare the anti-fouling behaviors of different polyelectrolytes (3D-PETx, 2D-PET, and PLL). Here, we first used bovine serum albumin (BSA), the major protein species found in bovine blood plasma as a template protein to evaluate the anti-fouling capability of the polyelectrolytes.

Fig. 5A shows the real time BSA adsorption on different polyelectrolytes. Glass fiber tip was first immersed in PETs (1 mg/mL) then BSA solution (15 μM). As compared in Fig. 5b, 2D-PET and 3D-PETx absorb much less BSA compared with PLL. It is noted that BSA hardly absorbs on 3D-PETx (30%) or 3D-PETx (40%) coated tips, proving their superior anti-fouling ability. We then tested the serum absorption on PLL, 2D-PET, and 3D-PETx (40%). The polyelectrolyte-modified fiber tips were incubated into serum with different dilutions (10%, 50% and 100%) for 5 min. Fig. 5C–E shows the wavelength shift as a function of time of serum adsorption on different polyelectrolytes initialized glass fiber tips using Blitz. As compared in Fig. 5F, 3D-PETx (40%) shows superior anti-fouling behavior. There is almost no absorption on 3D-PETx (40%) even with 100% serum. This is likely due to the high surface packing density of OEG component in 3D-PETx. As OEG and PLL are nontoxic and biocompatible polymers, which have been approved by the US Food and Drug Administration (FDA), we believe the 3D-PETx with super anti-fouling ability has potential for clinical sensing applications.

3.5. PSA detection in serum

As proved by the BSA and serum experiments, the 3D-PETx shows superior antifouling behavior, which is likely due to the enhanced surface density of the OEGs. We then tested the 3D-PETx coating for biomarker detection in complex matrices, which is a general issue in most of the label-free biosensing. Here, different concentrations of prostate-specific antigen (PSA), a typical clinically relevant target biomarker for prostate cancer (Li et al., 2019; Healy et al., 2007; Llop et al., 2016), were spiked in serum as a model system to study the immunosensing performance of 3D-PETx. Their sensing behavior were thoroughly compared with the 2D-PET. Unless otherwise specified hereinafter, 3D-PETx refers to 3D-PETx (40%).

It is interesting to note that though 3D-PETx shows superior anti-fouling behavior in the BioLayer Interferometry, the Blitz cannot obtain stable PSA adsorption signal in undiluted serum, which is likely due to the partial of the white light were scattered into the rather opaque and complex serum (Han et al., 2017). Only in diluted serum (10%), PSA absorption could be detected by Blitz (Fig. S11). Fig. S11A shows the monitored wavelength shift as a function of time for PSA detections with 3D-PETx and 2D-PET initialized glass fiber tips in 10% serum. As shown in Fig. S11B, 3D-PETx demonstrated stronger binding signals for PSA detection, especially at low concentration range.

To further investigate the PSA detection in undiluted serum condition, we used Surface Plasmon Resonance (SPR) as an alternative label-free sensing method, where the light beam is in total internal reflection and does not go through the solution. Such refractometric technique has been demonstrated to serve in complex matrices if an appropriate surface chemistry could protect the sensor against fouling (Bolduc et al., 2011; Bolduc et al., 2009; Aubé et al., 2016). Here, the SPR chips were functionalized with anti-PSA through PETs by the method mentioned above. PSA were spiked into undiluted serum with concentrations ranging from 0.6 ng/mL to 40 ng/mL and injected to the fresh coated SPR chips sequentially. Fig. 6A shows the SPR results for the detection of PSA in undiluted human serum. It is clearly noted that compared with the 2D-PET coating, the 3D-PETx coated chips show better sensitivity for PSA detection. Especially, the 3D-PETx coated chips present much stronger signals at low PSA concentration range (below 5 ng/mL), which is rather important for clinical PSA detection.

Besides label-free sensing, PSA detections were performed by regular ELISA as well. Anti-PSA was immobilized in each well by adding 50 μL PETs (1 mg/mL), SAv (200 nM) and biotinylated anti-PSA (200 μg/mL) subsequently and incubated in 96-well plates at room temperature for 20 min. Then, PSA solution of serial concentrations (0, 1, 4, 10, 25, 50 ng/mL) in human serum were tested with PETs coated plates. Fig. 6b shows that the light absorbance (ABS) at 450 nm against PSA concentration. Again, 3D-PETx coated substrate presents higher sensitivity (2.6 times) than 2D-PET coated. All the results prove that the 3D-PETx show better sensing performance in serum samples, which is due to its superior antifouling ability and higher probe density. The antigen detections in complex biological fluids with label-or label free techniques further demonstrate the potential of the 3D-PETx coating for real clinical applications.

4. Conclusions

In summary, we have demonstrated a novel 3D biosensor surface

based on pre-synthesized polyelectrolytes (3D-PETx) by grafting 2D PLL-g-OEG-biotin to a linear PLL using click chemistry. Compared with the 2D polyelectrolyte with chain-end biotin units, the 3D-PETx coating enables a thorns-like 3D sensor surface with enhanced antifouling and protein binding capacity due to the increased number of OEG and biotin sites per sensor surface unit. The grafting density was optimized to achieve optimal anti-fouling ability, protein sensing sensitivity, and surface binding stability. As a result, 3D-PETx (40%) provides an almost non-fouling surface even in undiluted human serum. In view of this, we demonstrated the PSA detection in serum with a LOD down to 0.6 ng/mL. Moreover, we proved that the 3D-PETx coated biosensor surface can be regenerated by pH stimulation, allowing repeated measurements when continuous monitoring of biomarkers is required (see supplementary information). Though here SAv-biotin was used as the linker, other bio-functional groups can be introduced as well for various targets. In future work, the graft ratio and chain length could be further optimized to reduce the crosslinks.

Considering the 3D-PETx coating can be simply achieved by dipping the sensor in the polymer solutions under room temperature, it provides a simple and reliable method for biosensor surface functionalization, which can be extended to various substrates and bioreceptors.

CRediT authorship contribution statement

Wenwei Pan: Methodology, Investigation, Writing - original draft. **Ziyu Han:** Investigation. **Ye Chang:** Investigation. **Xuexin Duan:** Conceptualization, Supervision, Writing - review & editing.

Declaration of competing interest

The authors declare that they have no known competing financial interests or personal relationships that could have appeared to influence the work reported in this paper.

Acknowledgements

The authors gratefully acknowledge financial support from the National Natural Science Foundation of China (NSFC No. 61674114, 91743110, 21861132001), National Key R&D Program of China (2017YFF0204604, 2018YFE0118700), Tianjin Applied Basic Research and Advanced Technology (17JCJQJC43600), the 111 Project (B07014), and the Foundation for Talent Scientists of Nanchang Institute for Micro-technology of Tianjin University.

Appendix A. Supplementary data

Supplementary data to this article can be found online at https://doi.org/10.1016/j.bios.2020.112504.

References

Albrecht-Schmitt, T., Bujoli, B., Cahill, C., Murugavel, R., Rocha, J., Hix, G., Winpenny, R., 2011. J. Roy. Soc.
Locke, Andrea K., Cummins, Brian.M., Abraham, Alexander.A., Coté, Gerard.L., 2015. Anal. Chem. 86, 9091–9097.
Aubé, A., Charbonneau, D.M., Pelletier, J.N., Masson, J.-F., 2016. ACS Sens. 1 (11), 1358–1365.
Bolduc, O.R., Clouthier, C.M., Pelletier, J.N., Masson, J.-F., 2009. Anal. Chem. 81 (16), 6779–6788.
Bolduc, O.R., Lambert-Lanteigne, P., Colin, D.Y., Zhao, S.S., Proulx, C., Boeglin, D., Lubell, W.D., Pelletier, J.N., Fethiere, J., Ong, H., Masson, J.F., 2011. Analyst 136 (15), 3142–3148.
Burg, T.P., Godin, M., Knudsen, S.M., Shen, W., Carlson, G., Foster, J.S., Babcock, K., Manalis, S.R., 2007. Nature 446 (7139), 1066–1069.
Chen, S., Zheng, J., Li, L., Jiang, S., 2005. J. Am. Chem. Soc. 127, 14473–14478.
Dieu, H.J.D., Jian, J., Xiulan, S., 2018. Anal. Lett. 51, 1–34.
Duan, X., Mu, L., Sawtelle, S.D., Rajan, N.K., Han, Z., Wang, Y., Qu, H., Reed, M.A., 2015. Adv. Funct. Mater. 25 (15), 2279–2286.
Gevrek, T.N., Kosif, I., Sanyal, A., 2017. ACS appl. Mater. Interfaces 9, 27946–27954.
Gregory, L., Kenausis, Vörös, J., Elbert, D.L., Huang, N., Hofer, R., Ruiz-Taylor, L., Textor, M., Hubbell, J.A., Spencer, N.D., 2000. J. Phys. Chem. B 104, 3298–3309.
Han, Z., Wang, Y., Duan, X., 2017. Anal. Chim. Acta 964, 170–177.
He, Y., Hower, J., Chen, S., Bernards, M.T., Chang, Y., Jiang, S., 2008. Langmuir 24 (18), 10358–10364.
Healy, D.A., Hayes, C.J., Leonard, P., McKenna, L., O'Kennedy, R., 2007. Trends Biotechnol. 25 (3), 125–131.
Howarter, J.A., Youngblood, J.P., 2006. Langmuir 22 (26), 11142–11147.
Iorio, D.D., Marti, A., Koeman, S., Huskens, J., 2019. RSC Adv. 9 (61), 35608–35613.
Jiang, B., Lian, L., Xing, Y., Zhang, N., Chen, Y., Lu, P., Zhang, D.Y., 2018. Environ. Sci. Pollut. R 25, 30863–30879.
Jonkheijm, P., Weinrich, D., Schröder, H., Niemeyer, C., Waldmann, H., 2008. Angew. Chem. Int. Ed. 47, 9618–9647.
Kingshott, P., Mcarthur, S., Thissen, H., Castner, D.G., Griesser, H.J., 2002. Biomaterials 23, 4775–4785.
Lange, S.C., Van Andel, E., Smulders, M.M.J., Zuilhof, H., 2016. Langmuir 32, 10199–10205.
Li, Z., Yin, J., Gao, C., Qiu, G., Meng, A., Li, Q., 2019. Sensor actuat. B-Chem. 295, 93–100.
Llop, E., Ferrer-Batallé, M., Barrabés, S., Guerrero, P.E., Ramírez, M., Saldova, R., Peracaula, R., 2016. Theranostics 6 (8), 1190.
Love, J.C., Estroff, L.A., Kriebel, J.K., Nuzzo, R.G., Whitesides, G.M., 2005. Chem. Rev. 105 (4), 1103–1170.
Marie, R., Beech, J.P., Vörös, J., Tegenfeldt, J.O., Höök, F., 2006. Langmuir 22 (24), 10103–10108.
Matta, L.L., Karuppuswami, S., Chahal, P., Alocilja, E.C., 2018. Biosens. Bioelectron 111, 152–158.
McKeating, K.S., Hinman, S.S., Rais, N.A., Zhou, Z., Cheng, Q., 2019. ACS Sens. 4 (7), 1774–1782.
Mcpartlin, D.A., Loftus, J.H., Crawley, A.S., Silke, J., Murphy, C.S., O'Kennedy, Richard, J., 2017. Curr. Opin. Biotechnol. 45, 164–169.
Morgenthaler, S., Zink, C., Städler, B., Vörös, J., Lee, S., Spencer, N.D., Tosatti, S.G., 2006. Biointerphases 1 (4), 156–165.
Park, J.W., Kim, H., Han, M., 2010. Chem. Soc. Rev. 39 (8), 2935–2947.
Prime, K.L., Whitesides, G.M., 1991. Science 252, 1164–1167.
Ruiz-Taylor, L.A., Martin, T.L., Zaugg, F.G., Witte, K., Indermuhle, P., Nock, S., Wagner, P., 2001. P. Natl. Acad. Sci. 98, 852–857.
Sappia, L., Felice, B., Sánchez, María A., Martí, Mercè, Pividori, I., 2018. Sensor. Actuator. B Chem. 281, 221–228.
Singh, A.K., Flounders, A.W., Volponi, J.V., Ashley, C.S., Wally, K., Schoeniger, J.S., 1999. Biosens. Bioelectron 14 (8–9), 703–713.
Srivastava, A.K., Dev, A., Karmakar, S., 2017. Environ. Chem. Lett. 16 (4), 1–22.
Veerbeek, J., Steen, R., Vijselaar, W., Rurup, W.F., Korom, S., Rozzi, A., Corradini, R., Segerink, L., Huskens, J., 2018. Langmuir 34, 11395–11404.
Wei, X.J., Zhang, Z.H., Wang, X.Q., Lenhart, B., Gambarini, R., Gray, J., Liu, C., 2020. Nanotechnol Precis Eng 3 (1), 2–8.
Wu, J.G., Chen, J.H., Liu, K.T., Luo, S.C., 2019. ACS appl. Mater. Interfaces 11 (24), 21294–21307.
Zhang, X., Yadavalli, V.K., 2011. Biosens. Bioelectron. 26 (7), 3142–3147.
Zhao, H., Zhu, B., Luo, S.C., Lin, H.A., Yu, H.H., 2013. ACS appl. Mater. Interfaces 5, 4536–4543.
Zhao, S.S., Bukar, N., Toulouse, J.L., Pelechacz, D., Robitaille, R., Pelletier, J.N., Masson, J.-F., 2015. Biosens. Bioelectron. 64, 664–670.
Zhen, G., Eggli, V., Vörös, J., Zammaretti, P., Textor, M., Glockshuber, R., Kuennemann, E., 2004. Langmuir 20 (24), 10464–10473.